JMEPEG (2010) 19:325–334
DOI: 10.1007/s11665-009-9510-y
©ASM International
1059-9495/$19.00

Investigation of the Hot-Stamping Process for Advanced High-Strength Steel Sheet by Numerical Simulation

H.S. Liu, Z.W. Xing, J. Bao, and B.Y. Song

(Submitted August 28, 2008; in revised form June 9, 2009)

Hot forming is a new way to manufacture complex-shaped components of advanced high-strength steel (AHSS) sheet with a minimum of spring-back. Numerical simulation is an effective way to examine the hot-forming process, particularly to determine thermal and thermo-mechanical characteristics and their dependencies on temperature, strain and strain rate. The flow behavior of the 22MnB5 AHSS is investigated through hot tensile tests. A 3D finite element (FE) model of hot-stamping process for the ⌝⌜ shaped part is built under the ABAQUS/Explicit environment based on the solutions of several key problems, such as treatment of contact between blank and tools, determination of material characteristics and meshing, etc. Numerical simulation is carried out to investigate the influence of blank holder force (BHF) and die gap on the hot-forming process for the ⌟ shaped part. Numerical results show the FE model is effective in simulation of hot-forming process. Large BHF reduces the amount of spring-back and improves the contact of flange with tools while avoiding cracking of stamped part. Die gap has a considerable influence on the distribution of temperature on side walls; the larger the die gap, higher is the temperature on the sidewall of ⌟ shaped part.

Keywords advanced high-strength steel, finite element, hot stamping, simulation, spring-back

1. Introduction

In the last decade, the most challenging goals in automotive industry have been (i) the increase of crash performance and safety, (ii) the reduction of automotive weight and fuel consumption, and (iii) the increase of accuracy and precision for easy, cheap and reliable joining and assembly. Although the application of aluminium sheets to automobile parts is attractive for the reduction in weight, high cost and low formability are crucial problems which are difficult to solve, and thus the industry still has a great interest in steel sheets (Ref 1). Steel sheet with tensile strength exceeding 800 MPa has been developed in recent years. In 1994, a consortium of 35 companies participated in a worldwide co-operative project known as ULSAB (Ultra Light Steel Auto Body) coordinated by the international iron and steel institute (visit www.worldautosteel.org for further information). Since the ULSAB project was advanced, the use of advanced high-strength steel (AHSS) sheets for automobile body panels has rapidly increased. However, reduced formability and the tendency toward spring-back still pose challenges for further application of AHSS sheet metal in automotive industry (Ref 2). Studies have focused on room temperature stamping of AHSS sheet metal; for example, in Ref 3, the influence of low-strain deformation characteristics of high-strength sheet steel on curl and spring-back in bend-under-tension tests was investigated, and the effect of yielding and work hardening on curl and spring-back were examined and explained. In Ref 4, the variation of spring-back after room temperature forming of AHSS sheet metal was predicted through numerical simulations. In order to accurately model AHSS sheet metal forming, experimentally reliable benchmarks were used to determine the fundamental behavior of material (Ref 5). However, the tendency for spring-back and the low formability are the main problems associated with the room temperature forming of AHSS sheet metal.

To improve part formability and extend the application of AHSS sheet metal, new forming technologies such as hot stamping were developed. Hot forming is a non-isothermal process in which forming and quenching occur concurrently in a single step. Hot forming improves the formability of AHSS sheet metal, sharply reduces the deformation resistance and the amount of spring-back, and improves the elongation of AHSS sheet metal at elevated temperatures (Ref 6). Figure 1 schematically illustrates the hot-stamping process. The initial austenitic microstructure is transformed into martensitic microstructure prior to hot stamping and the tensile strength of hot stamped part increases sharply. Spring-back influences the shape precision of stamped part and is predicted with the help of elastic and viscoplastic crystal plasticity models for polycrystalline high-strength low-carbon steel (Ref 7). The influence of the forming temperature on spring-back has been examined and the appropriate forming temperature is reported to be more than 750 °C (Ref 8). The mechanism of spring-back after hot forming under warm forming conditions has been investigated and the main factors influencing the amount of spring-back have been examined (Ref 9).

In order to determine the mechanical and microstructure characteristics of sheets at elevated temperature, a novel test

H.S. Liu, Z.W. Xing, J. Bao, and **B.Y. Song**, School of Mechatronics Engineering, Harbin Institute of Technology, P.O. Box 425, No. 92, West Da-Zhi Street, Harbin 150001, P.R. China. Contact e-mail: hs_liu_hit@163.com.

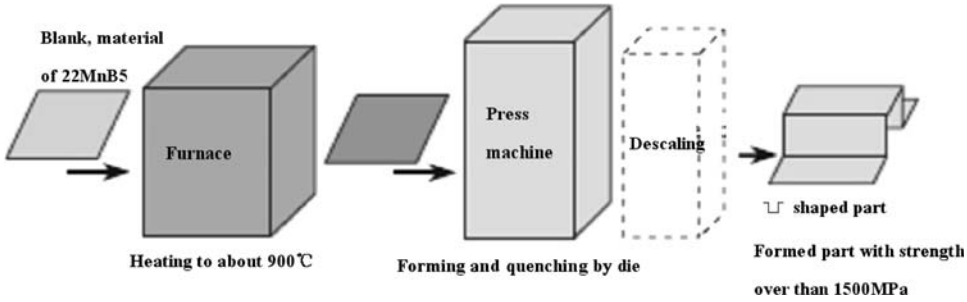

Fig. 1 Hot-stamping process of AHSS sheet metal for ⊔ shaped part

based on Nakazima concept (Ref 10) was presented to evaluate the material formability at elevated temperature (Ref 11). Hot forming is a complicated process and involves material nonlinearity, geometric nonlinearity, nonlinearity of contact and the dependencies of thermo-mechanical properties on temperature. Thus, it is difficult to solve the problems involved in practical hot stamping exactly and effectively only by using analytical methods and the experiments. Up until now, powerful numerical simulation techniques do not appear to have been employed to investigate the hot forming process and optimize the processing parameters.

In this paper, 22MnB5 steel is selected as AHSS, and the finite element (FE) simulation is employed to study the hot forming of 22MnB5 AHSS sheet metal through solutions of several key problems. To build a 3D elastoplastic thermo-dynamic FE model where both computational cost and the accuracy of numerical simulation are considered, reasonable solutions of the key problems, such as treatment of contact boundary conditions, determination of material properties and meshing, etc., are presented. In order to determine the thermal and thermo-mechanical characteristics of 22MnB2 AHSS, the flow behavior of the material in the austenitic state is investigated by hot tensile tests as well as modeled by mathematical methods. The type of mesh used in the numerical model is selected as CPE4RT, and penalty method is employed to treat the contact between tools and blank. Based on the above approach, a numerical model is developed to carry out the numerical simulations for ⊔ shaped part. The influence of two main processing parameters, namely blank holder force (BHF) and die gap, is examined.

2. FE Modeling of Hot-Stamping Process of AHSS Sheet Metal for ⊔ Shaped Part

2.1 Definition of Material Properties for Hot-Stamping Process

With regard to reliable modeling and numerical simulation of hot-stamping process, besides the determination of the tribological conditions and the mechanical characteristics, the knowledge of thermal and thermo-mechanical material properties and their dependencies on the time-temperature characteristic of the hot-stamping process is required. Hot tensile tests are performed at different temperatures and strain rates to investigate thermal and thermo-mechanical flow properties of 22MnB5 AHSS with the aid of a mechanical Gleeble 1500 testing system. First, the specimens are austenitized at 900 °C

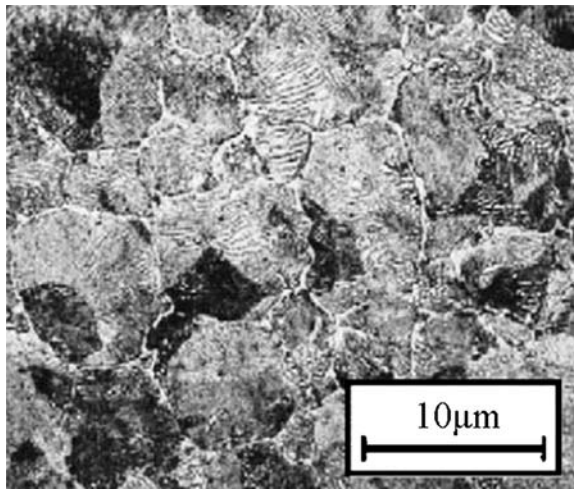

Fig. 2 Austenitic microstructure through austenitization

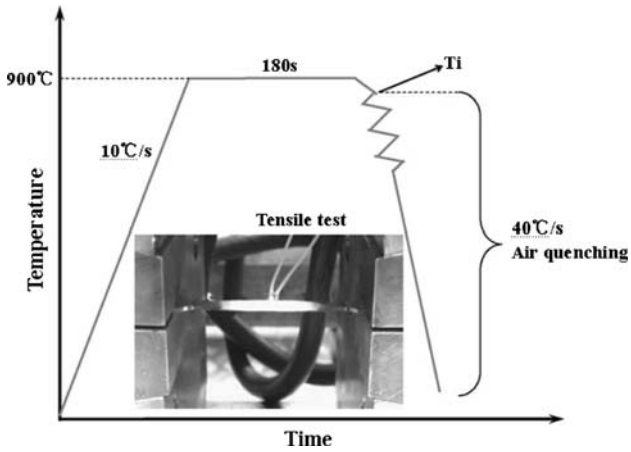

Fig. 3 Thermo-mechanical cycle for tensile testing and tensile specimen during a heating test

for 180 s (Fig. 2), cooled in air for a few seconds to reproduce the heat loss during the transfer to the press, and then subjected to a cooling rate equal to 40 °C/s to avoid the bainite transformation. Once the chosen testing temperature is reached, uni-axial tensile tests are carried out while continuing to quench the specimen. The temperature versus time diagram of the tensile test is shown in Fig. 3. The specimen's geometry follows the recommendation of EN482-2 (Ref 12).

The deformation of the specimens is detected using the optical measuring system ARAMIS. The final calculation of the true stress and strain values follows Ref 13. Metallographic observations are carried out to confirm that all the specimens presented a fully martensitic microstructure at the end of the test.

The influence of the temperature on flow stress of AHSS sheet metal is investigated under different temperatures from 600 to 850 °C and strain rates of 0.01, 0.1 and 1.0 s^{-1}. Figure 4 shows the true stress-true strain curves at different temperatures of 600, 750 and 850 °C with the strain rate of 0.01 s^{-1}. It can be seen from Fig. 4 that temperature has a significant influence on the flow stress of AHSS sheet metal, and increasing temperature leads to the decrease in the flow stress and work hardening as well as hardening exponent. According to the results shown in Fig. 5, besides the temperature, the strain rate influences the flow properties of AHSS sheet metal and has thus to be considered in characterizing the material properties.

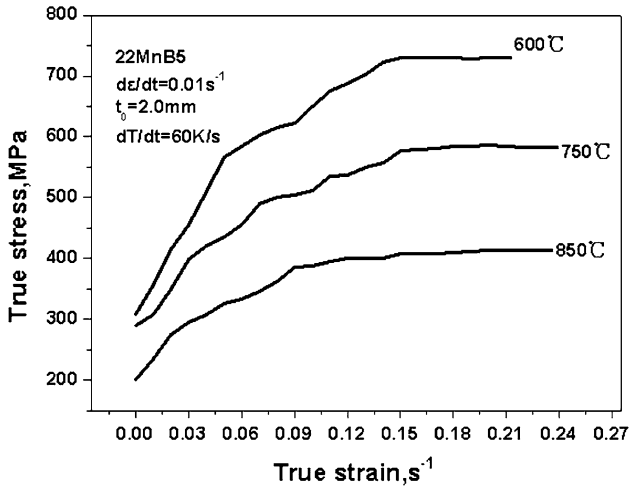

Fig. 4 Influence of the temperature on flow curve properties of AHSS at strain rate of 0.01 s^{-1}

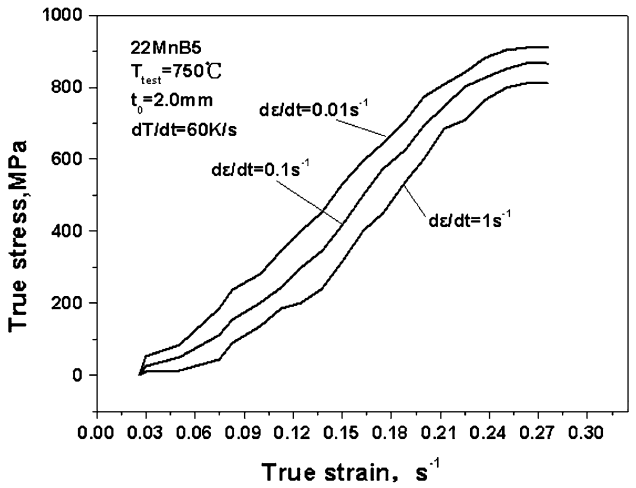

Fig. 5 Influence of strain rate on flow curve properties of AHSS at temperature of 750 °C

The dependency of the flow behavior of material on the strain rate is investigated at different strain rates of 0.01, 0.1 and 1.0 s^{-1} after rapid cooling in the austenitic state. In Fig. 5, the dependency of strain hardening on strain rate is shown. For each strain rate, a representative flow curve is displayed. According to the characteristics of the curve, it is apparent that the strain rate has a significant influence on the flow stress of the material, and increasing strain rate leads to a considerable increase in flow stress and an appreciable increase of stress level as well as the slope of the curve as a consequence of enforced work hardening of the material. Further, it can be seen that the flow curves exhibit a tendency to achieve a steady state after the initial strain hardening. This leads to an almost asymptotic trend of the strain hardening function with progressive elongation, and thus the crack could be avoided even though larger deformation took place during hot stamping. A multi-variant linear regression based on least square methodology is used to describe the material's rheological behavior as a function of strain, strain rate and temperature by fitting experimental datum through the software OriginPro 7.5, and the constitutive equation of AHSS sheet metal is obtained and expressed as

$$\sigma = K\varepsilon^n \dot{\varepsilon}^m \exp(\beta/T) \quad \text{(Eq 1)}$$

where K = 15.23, n = 0.429, m = 0.1479, and β = 3509.2.

2.2 Analysis Steps

A schematic view of die, punch, blank holder and blank used in the hot-stamping process is shown in Fig. 6. The hot-stamping process consists of the following four forming steps shown schematically in Fig. 7: (a) exerting BHF on the blank holder (during this process, blank holder moves down and keeps contact with blank); (b) hot stamping (during this process, punch moves down and the material of the flange flows into the die cavity with die and blank holder remaining stationary); (c) quenching of stamped part (during this process, the stamped part dwells in die cavity for about 6 s, and within this time, the stamped part cools rapidly); and (d) spring-back (during this process, tools move away from stamped part and spring-back takes place). According to the hot-forming steps, the FE numerical simulation procedure of the hot-stamping process for ⊔ shaped part consists of the following corresponding computational steps: (a) applying BHF; (b) numerical computation of hot-forming process; (c) numerical computation of cooling or quenching; and (d) numerical prediction of spring-back. An extremely small velocity of moving away from the blank is applied on the punch in the analysis of spring-back to reduce nonlinearity of dynamic contact and thus to predict the amount of spring-back exactly. Timeslices used in each computational step are as follows: timeslice between 0 and 0.0001 s used in applying BHF, timeslice between 0.0001 and 0.9001 s used in analysis of hot stamping, timeslice between 0.9001 and 6.9001 s used in analysis of quenching and timeslice between 6.9001 and 10.7001 s used in analysis of spring-back.

2.3 Determination of Thermophysical Parameters Involved in Hot Stamping

Thermophysical parameters of 22MnB5 AHSS, such as heat conductivity, thermal expansion and specific heat, etc., are essential for numerical simulation of hot-stamping process of

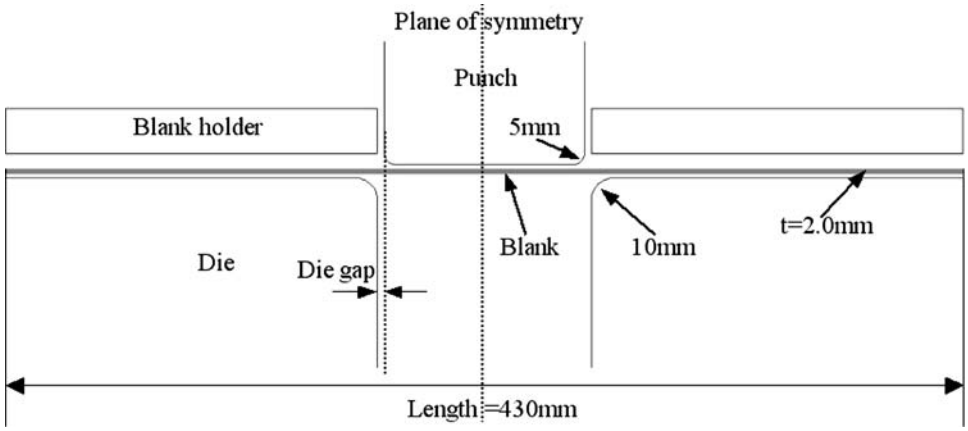

Fig. 6 Schematic illustration of tools and blank used within hot-stamping process

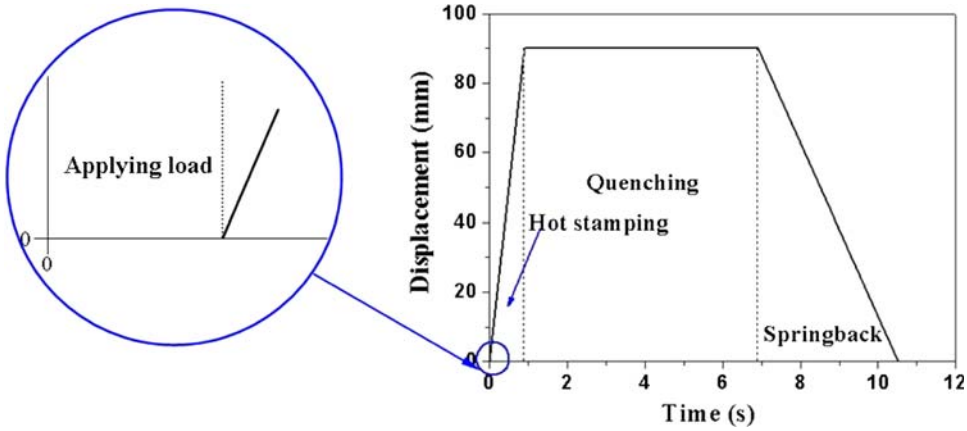

Fig. 7 Forming steps, computational steps and displacement of punch as time increases

Table 1 Coefficients of heat conduction at different temperatures

Temperature, °C	100	200	300	400	450	650	800	900
Heat conduction, W/m·K	10.88	9.97	9.49	8.58	7.91	5.32	5.53	5.43

Table 2 Specific heats at different temperatures

Temperature, °C	50	100	200	300	400	850	900	950
Specific heat, J/kg·K	465	471	466	459	479	987	1019	1062

AHSS sheet metal. During hot stamping, the blank maintains contact with die, punch and blank holder, and heat is transferred from the blank to the tools; simultaneously the blank get cooled and quenched. Heat conductivity has an important influence on effectiveness of quenching. Thermal expansion affects thermal contraction and therefore the accuracy of formed part shape. In order to build the numerical model of hot-stamping process, heat conductivity, thermal expansion and specific heat of AHSS blank should be determined exactly at different temperatures. In this paper, heat conductivity, thermal expansion and specific heat are determined through thermal tests and are listed in Table 1, 2, and 3, respectively.

Table 3 Coefficients of thermal expansion at different temperatures

Temperature, °C	50	100	200	300	400	850	900	950
Thermal expansion, /°C × 10^{-5}	1.89	1.93	1.97	2.12	2.17	2.62	2.78	3.08

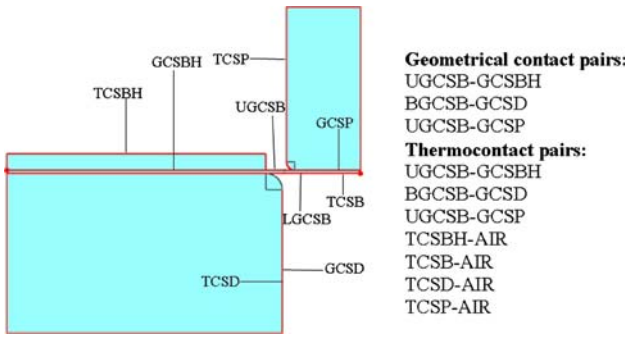

Fig. 8 Definition of contact surfaces and contact pairs

2.4 Definition of Contact Surfaces

The surfaces of tools and blank must be defined in order to treat the contact involved in numerical simulation of hot forming. Compared with room temperature stamping, besides geometrical contact, the contact surfaces involved in hot stamping include as well thermal contact. There are five geometrical contact surfaces in hot-stamping process for ⊔ shaped part, which are geometrical contact surface of die (GCSD), geometrical contact surface of punch (GCSP), geometrical contact surface of blank holder (GCSBH), upper geometrical contact surface of blank (UGCSB) and lower geometrical contact surface of blank (LGCSB) illustrated in Fig. 8. In order to treat thermal contact exactly, other four surfaces in contact with air need to be defined; these are thermal contact surface of die (TCSD), thermal contact surface of punch (TCSP), thermal contact surface of blank holder (TCSBH) and thermal contact surface of blank (TCSB) shown in Fig. 8. Contact pairs are defined and shown in Fig. 8. In the hot-stamping process, for different contact surfaces, the corresponding ways of transferring heat are different. The formula for describing the heat transference from blank to tools is expressed as

$$q_d = h_{lub}(T - T_t) \quad \text{(Eq 2)}$$

where h_{lub} is the coefficient of heat conduction, T_t is the temperature on tools, T is the temperature on blank. The

Table 4 Main parameters used in hot stamping for ⊔ shaped part

Geometrical parameters of blank	
Length	430 mm
Width	200 mm
Thickness	2 mm
Punch stroke	90 mm
Coefficient of friction	0.8
Temperature of air	25 °C
Forming temperature	900 °C
Density	7800 kg/m^3
Poisson's ratio	0.28
Punch profile radius	5 mm
Die profile radius	10 mm

Table 5 Young's modulus at different temperatures

Temperature, °C	20	200	400	600	800	900
Young's modulus, GPa	502	494	487	482	478	473

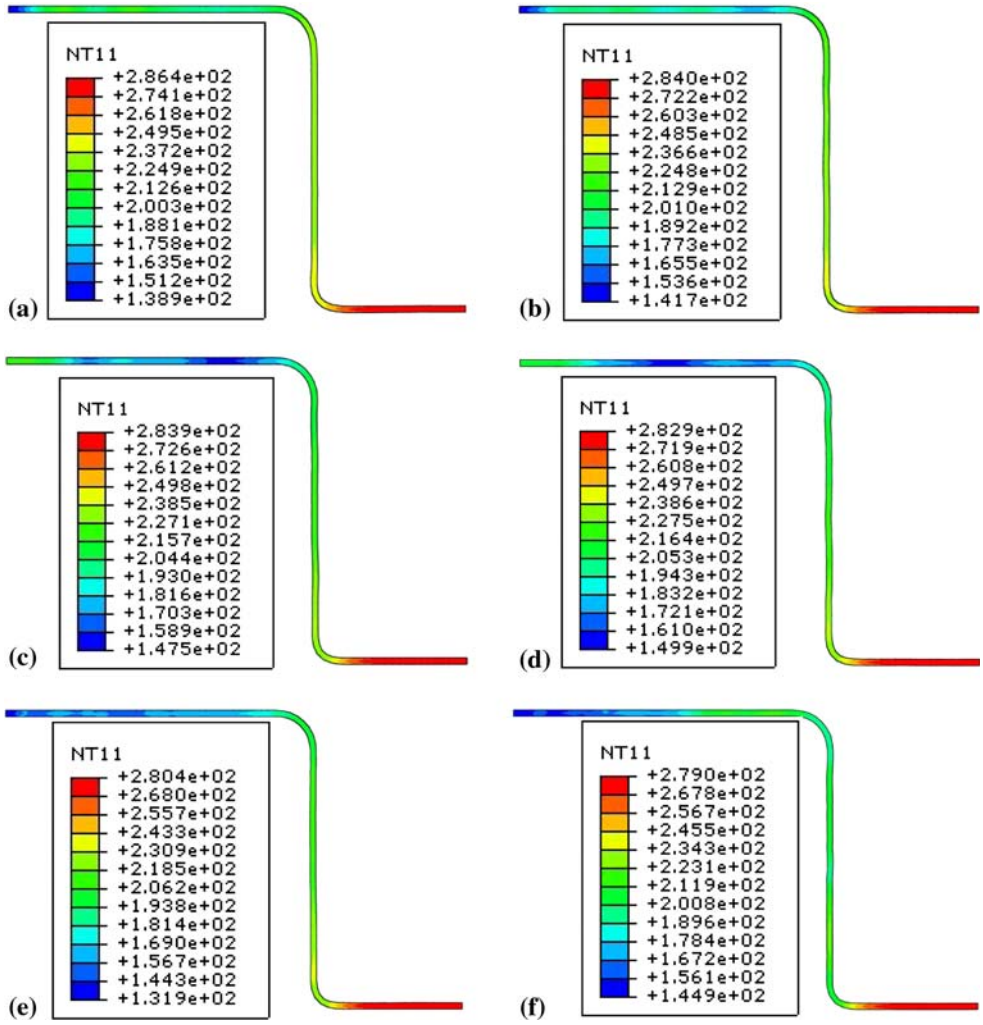

Fig. 9 Distribution of temperature for different BHFs. BHF = 1.0 MPa (a), 1.5 MPa (b), 2.0 MPa (c), 2.5 MPa (d), 3.0 MPa (e), and 3.5 MPa (f)

formula for describing heat transfer from blank to air is expressed as

$$q_c = h_c(T - T_\infty) \quad \text{(Eq 3)}$$

where h_c is the coefficient of convective heat exchange, T_∞ is the temperature of air and T is the temperature of blank.

2.5 Preprocessing for Numerical Simulation of Hot Forming

Due to symmetry, one half of the numerical model is selected to reduce computational efforts, and the assembly of die, punch, blank holder and blank is shown in Fig. 8. Treatment of boundary constrains and loading is implemented

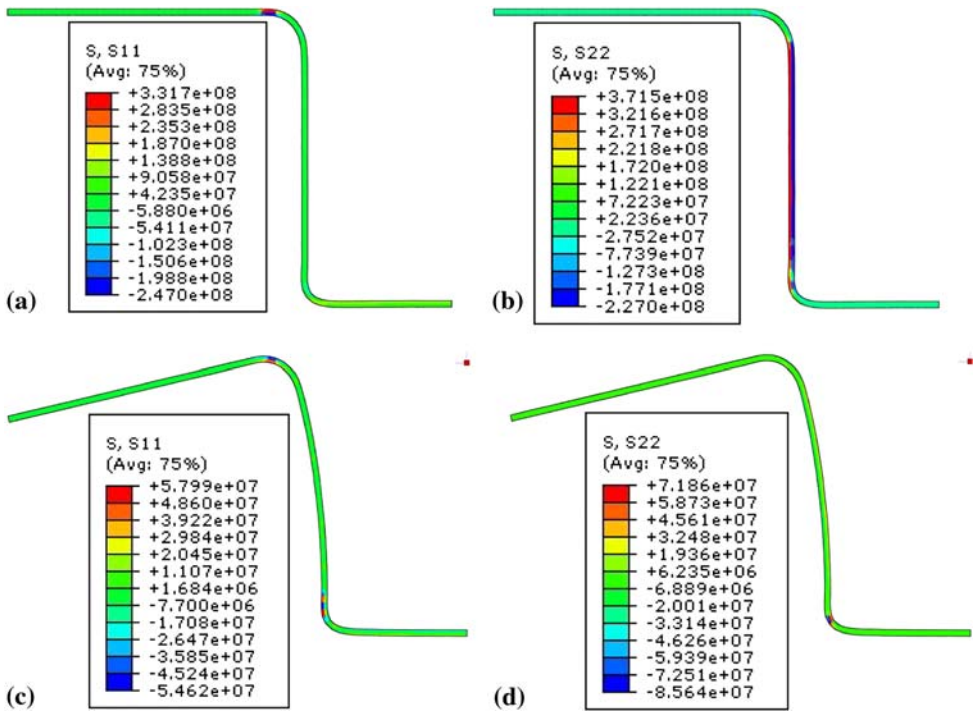

Fig. 10 Distribution of σ_x and σ_y at the end of quenching and after spring-back for BHF of 1.0 MPa. Distribution of (a) σ_x and (b) σ_y at the end of quenching. Distribution of (c) σ_x and (d) σ_y after spring-back

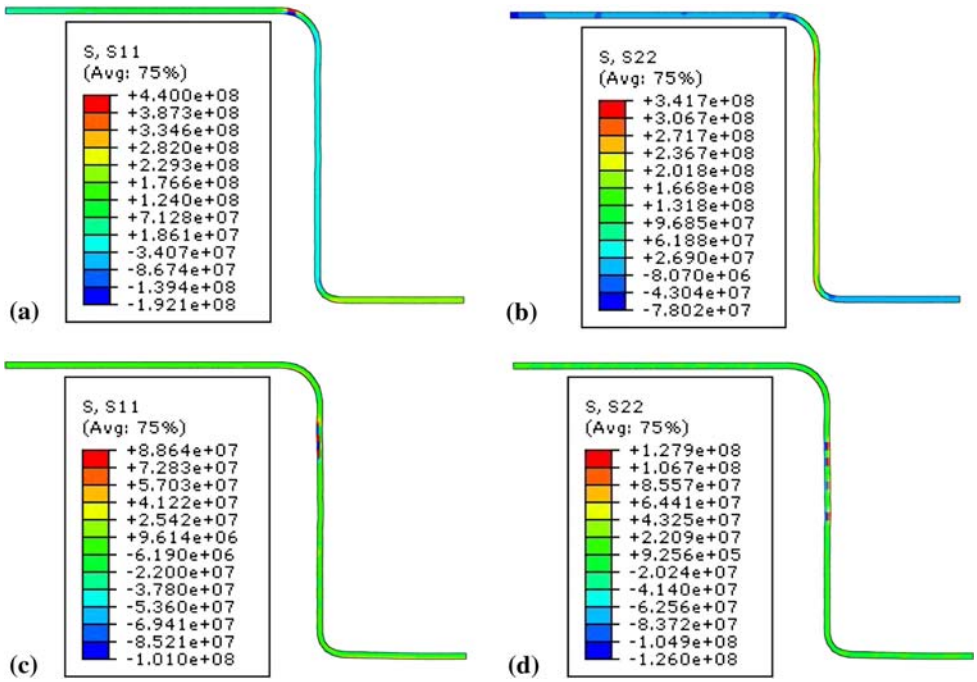

Fig. 11 Distribution of σ_x and σ_y at the end of quenching and after spring-back for BHF of 3.5 MPa. Distribution of (a) σ_x and (b) σ_y at the end of quenching. Distribution of (c) σ_x and (d) σ_y after spring-back

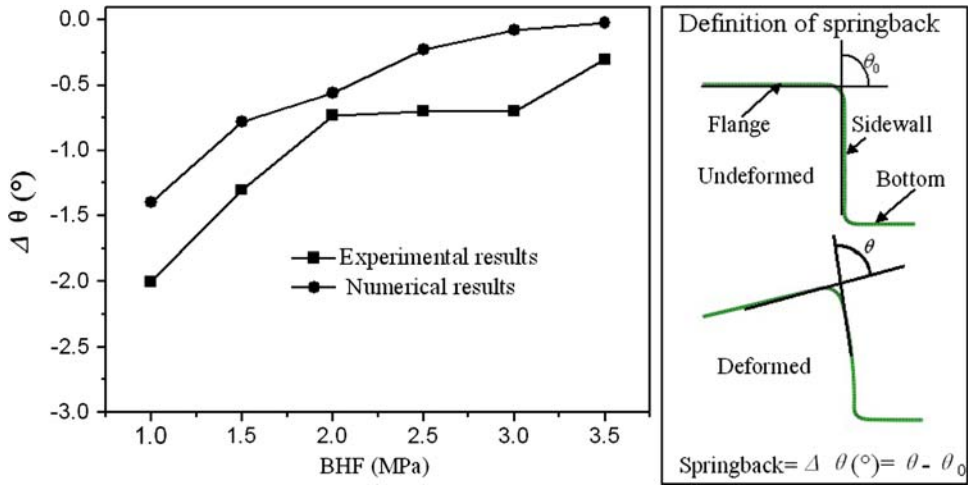

Fig. 12 Variation of spring-backs Δθ (°) as BHF increasing and definitions of spring-back on ㄱ shaped part

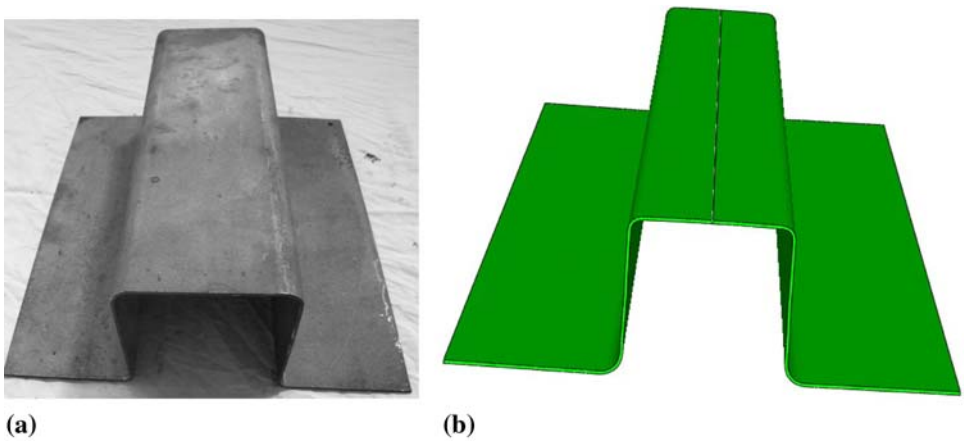

Fig. 13 ㄱ shaped part formed by experiment for the die gap of 2.4 mm and the BHF of 2.4 MPa. (a) Experimental result; (b) numerical result

through the mode of displacement/rotation. During the hot-stamping process, die is fixed and the punch moves down for a prescribed punch stroke within a prescribed timeslice in the direction of *y* and remains stationary in the direction of *x*. The displacement of punch-time curve and four computational steps are shown in Fig. 7. The blank holder is fixed in the *x* direction and movable in the *y* direction. Initial temperature of bodies is prescribed as 25 °C prior to hot forming. The mesh of CPE4RT (4-node plane strain thermally coupled quadrilateral, bilinear displacement and temperature, reduced integration, hourglass control) is selected to discretize the blank, punch, the die and the blank holder in the FE model of hot-stamping process.

3. Numerical Simulation of Hot Forming for ㄷ Shaped Part

3.1 Conditions of Numerical Simulation

The processing parameters, such as heat conduction, specific heat and thermal expansion at different temperatures used in the hot-stamping process, are listed in Table 1, 2 and 3, respectively. Other processing parameters and the parameters characterizing the material performance used in the hot-stamping process are listed in Table 4. The constitutive equation of the material is expressed in Eq 1. The Young's

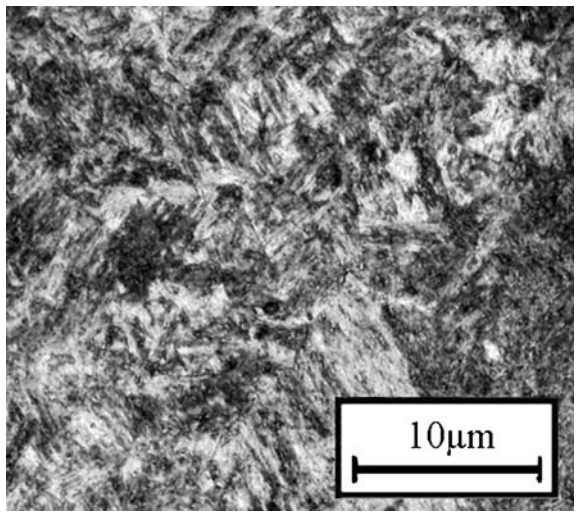

Fig. 14 Microstructure on side wall at the end of quenching for die gap of 3.0 mm

modulus of 22MnB5 AHSS sheet metal at different temperatures is listed in Table 5. The influences of two main processing parameters on hot-forming process are investigated for different BHFs and die gaps through FE numerical simulations.

3.2 Numerical Results and Discussion

3.2.1 Influence of BHF on Hot Forming. The influence of BHF on spring-back is investigated for different BHFs through FE numerical simulations with the prescribed die round radius of 10.0 mm and die gap of 3.0 mm. Figure 9 shows the distribution of temperature on ⊔ shaped part at the end of quenching for different BHFs from 1.0 to 3.5 MPa. It could be seen from the distribution of temperature on the stamped part shown in Fig. 9 that the temperature on the ⊔ shaped part is decreasing from the left of the flange to the bottom and the BHF has a significant influence on the distribution of temperature. The main cause for this is that the amount of BHF has a significant influence on the contact of the flange with blank holder and die. The higher the BHF, the better is the contact between tools and the flange. It is apparent that the good contact between blank and tools facilitates the heat transference from blank to the die and the blank holder, and according to the results shown in Fig. 9, the temperature on the left of the flange is lower than that on the right of the flange with BHF increasing. The bottom of ⊔ shaped part is slightly vaulted and deviated away from punch; this leads to poor contact between bottom and punch, and therefore restrains the heat transference from the bottom to the tools and leads to the highest temperature on the bottom of ⊔ shaped part.

For two different BHFs of 1.0 and 3.5 MPa, the distributions of stress σ_x and σ_y at the end of quenching and after spring-back are displayed in Fig. 10 and 11, respectively. It could be seen from Fig. 10 that a large amount of spring-back

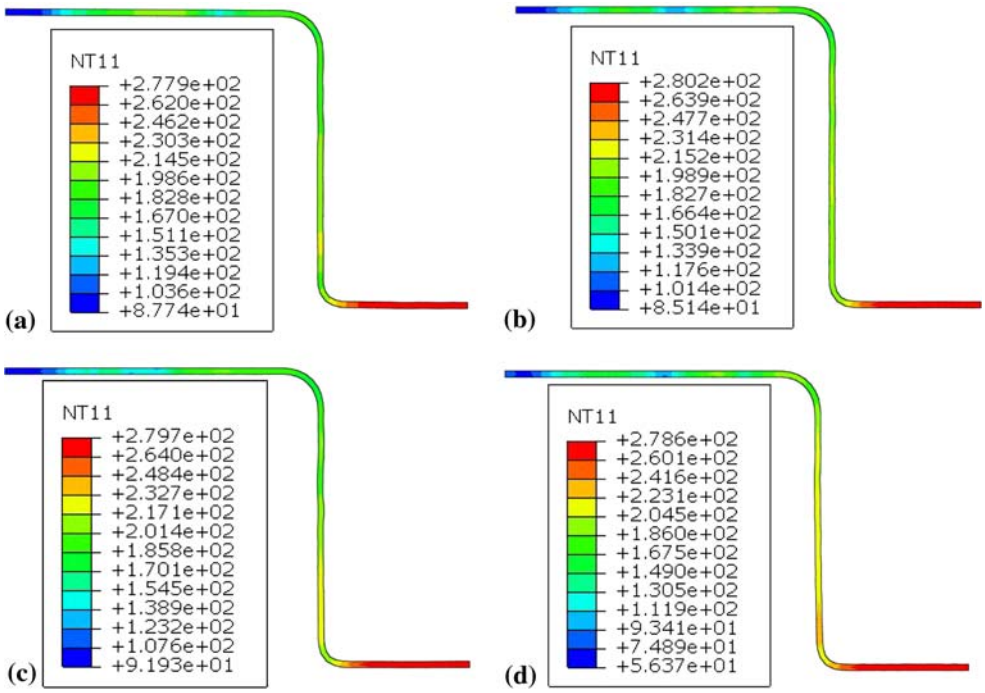

Fig. 15 Distribution of temperature on ⊔ shaped part for different die gaps. Die gap = 2.005 mm (a), 2.025 mm (b), 2.5 mm (c), and 3.0 mm (d)

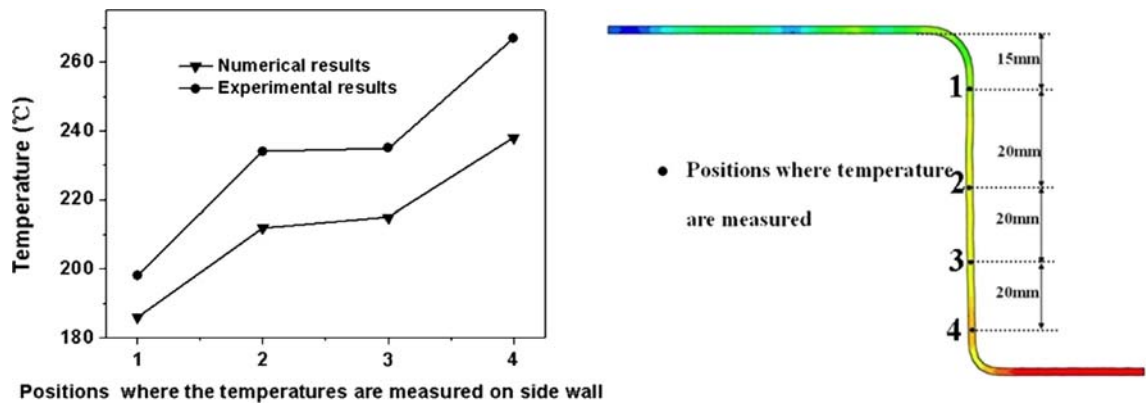

Fig. 16 Comparison of distribution of temperature obtained through experiment and numerical simulation

takes place after quenching. The main cause is that the non-uniform distribution of temperature on stamped part results in the non-uniform distribution of stress, which is the origin of residual stress. The residual stress is released to thus result in the spring-back after hot-stamping process. It should be noted that the spring-back after hot stamping has a direct relationship with the angle θ shown in Fig. 12 and is different from that after room temperature stamping. The spring-back Δθ is negative in the hot-stamping process, but for the room temperature stamping the spring-back Δθ is positive. Applying larger BHF of 3.5 MPa on the blank holder leads to a noticeable decrease in spring-back shown in Fig. 11. The main cause for this is that the distribution of temperature on the flange and the sidewall is getting more and more uniform with BHF increasing shown in Fig. 9. The uniform distribution of stress helps to decrease the residual stress and thus spring-back. According to the comparison of numerical results with experimental results shown in Fig. 12, it can be seen that the numerical results are in good agreement with experimental results. Figure 13 shows the ㄱ shaped part obtained through hot-stamping experiment with die gap of 2.4 mm and BHF of 3.5 MPa and the ㄴ shaped part obtained by numerical simulation. It can be also seen from Fig. 13 that the amount of spring-back is very small and the numerical result has good agreement with experimental result.

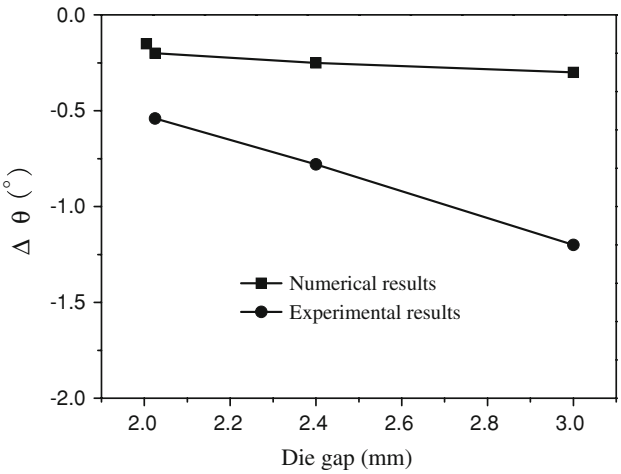

Fig. 17 Variation of spring-backs Δθ (°) as die gap increases

3.2.2 Influence of Die Gap on Hot Forming. The sidewall of the ㄱ shaped part cannot be cooled and quenched fully due to the die gap, so the initial austenitic microstructure on the sidewall cannot be transformed into martensitic microstructure completely at the end of quenching. Actually, the microstructure of sidewall is the mixture of martensite and bainite as shown in Fig. 14 at the end of quenching. The influence of die gap on the distribution of temperature on the sidewall is investigated through numerical simulations and experiments. Figure 15 shows the distribution of temperature on the sidewall at the end of quenching for different die gaps. Figure 16 shows the temperatures at several positions on sidewall obtained by numerical simulations and experiments.

According to the results shown in Fig. 15 and 16, a decrease of die gap improves the contact of the sidewall with punch and die, and thus decreases the temperature on the sidewall. It can be seen from Fig. 16 that the numerical results are in good agreement with experimental results. Thus, the sidewall can be quenched fully with a decrease of die gap. The influence of die gap on the spring-back is investigated by numerical simulation and experiments. It could be seen from Fig. 17 that the tendency of variation in spring-back with increasing die gap obtained by numerical simulation is consistent with that obtained by experiments. The distribution of temperature in die is examined through numerical simulations and is shown in Fig. 18. The distribution of temperature in die by numerical simulation is compared with that by experiment. Figure 18 shows that the prediction of temperature distribution in die is reliable.

4. Conclusions

Based on the numerical model developed for simulating the hot-forming process in this paper, the following main contribution of this paper and conclusions can be drawn:

(1) Several key problems involved in the numerical simulation of the hot-stamping process of AHSS sheet metal, such as definition of the AHSS material characteristic, treatment of contact and meshing etc., are solved successfully. The material characteristic of AHSS sheet

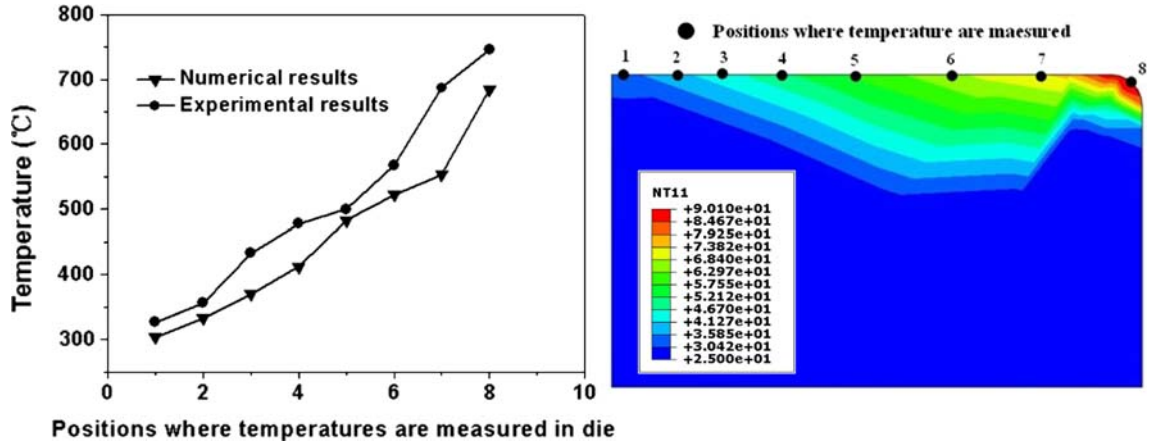

Fig. 18 Comparison of distribution of temperature in die obtained by numerical method with that by experiments

metal is determined by hot tensile tests under different temperatures and strain rates as well as characterized by the constitutive equation obtained by fitting experimental results through multivariant linear regression. The material constitutive equation plays an important role in numerical simulation of hot-forming process. Based on the above work a reliable numerical model of hot-stamping process is developed.

(2) Numerical simulation of hot-stamping process of AHSS sheet metal for ㄩ shaped part has been carried out by using the numerical model to investigate the influence of two important processing parameters, namely blank holder force and die gap on hot-stamping process. It can be concluded from the numerical results and the comparisons of numerical results with experimental results that large BHF helps to reduce the amount of springback and improves the contact of flange with tools while avoiding the crack on stamped part during the hot-forming process. Die gap has a considerable influence on the distribution of temperature on the sidewall of ㄩ shaped part. The larger the die gap, the higher is the temperature on the sidewall of ㄩ shaped part. The good agreement between numerical results and experimental results shows the effectiveness of the numerical model of hot-stamping process of AHSS sheet metal and that the numerical model is reliable in numerical analysis of hot-stamping process.

Acknowledgment

The authors acknowledge M.S. Sun Guiqing of Harbin Institute of Technology for his fruitful advices on the experiments of hot forming of HSS sheet metal for ㄱㄷ shaped parts.

References

1. K. Mori, K. Akita, and Y. Abe, Springback Behavior in Bending of Ultra-High-Strength Steel Sheets Using CNC Servo Press, *Int. J. Mach. Tools Manuf.*, 2007, **47**, p 321–325
2. J.X. Lu and L. Wang, Production and Usage of High Strength Sheet Metal Used in Automotive Industry, *Automob. Technol. Mater.*, 2004, **2**, p 1–6 (in Chinese)
3. P. Chen and M. Koc, Simulation of Springback Variation in Forming of Advanced High Strength Steels, *J. Mater. Process. Technol.*, 2007, **190**, p 189–198
4. T.B. Hilditch, J.G. Speer, and D.K. Matlock, Influence of Low-Strain Deformation Characteristics of High Strength Sheet Steel on Curl and Springback in Bend-Under-Tension Tests, *J. Mater. Process. Technol.*, 2007, **182**, p 84–94
5. A.D. Santos and P. Teixeirab, A Study on Experimental Benchmarks and Simulation Results in Sheet Metal Forming, *J. Mater. Process. Technol.*, 2008, **199**(3), p 327–336
6. K. Mori, S. Maki, and Y. Tanaka, Warm and Hot Stamping of Ultra High Tensile Strength Steel Sheets Using Resistance Heating, *Ann. CIRP*, 2005, **54**, p 209–212
7. S.H. Choi and K.G. Chin, Prediction of Spring-Back Behavior in High Strength Low Carbon Steel Sheets, *J. Mater. Process. Technol.*, 2006, **171**, p 385–392
8. J. Yanagimoto, K. Oyamada, and T. Nakagawa, Springback of High-Strength Steel After Hot and Warm Sheet Formings, *CIRP Ann. Manuf. Technol.*, 2005, **54**(1), p 213–216
9. J. Yanagimoto and K. Oyamada, Mechanism of Springback-Free Bending of High-Strength Steel Sheets Under Warm Forming Conditions, *Ann. CIRP*, 2007, **56**(1)
10. T. Klikuma and K. Nakazima, Effect of Deforming Conditions and Mechanical Properties on the Stretch Forming Limits of Sheet, *IDDRG, Tokyo 1970—Proceeding of ICSTIS, Trans. ISIJ*, 1971, p 827–831
11. A. Turetta, S. Bruschi, and A. Ghiotti, Investigation of 22MnB5 Formability in Hot Stamping Operations, *J. Mater. Process. Technol.*, 2006, **177**, p 396–400
12. Europaische Norm EN485-2
13. H. Hoffmann and C. Vogl, Determination of True Stress–Strain-Curves and Anisotropy in Tensile Test with Optical Deformation Measurement, *Ann. CIRP*, 2003, **52**(1), p 217–220